JACS
JOURNAL OF THE AMERICAN CHEMICAL SOCIETY
Communication
pubs.acs.org/JACS

Octahedral Pd@$Pt_{1.8}$Ni Core–Shell Nanocrystals with Ultrathin PtNi Alloy Shells as Active Catalysts for Oxygen Reduction Reaction

Xu Zhao,[†] Sheng Chen,[†] Zhicheng Fang,[†] Jia Ding,[†] Wei Sang,[†] Youcheng Wang,[†] Jin Zhao,[†] Zhenmeng Peng,*[,‡] and Jie Zeng*[,†]

[†]Hefei National Laboratory for Physical Sciences at the Microscale & Synergetic Innovation Center of Quantum Information and Quantum Physics, Center of Advanced Nanocatalysis, and Department of Chemical Physics, University of Science and Technology of China, Hefei, Anhui 230026, P. R. China

[‡]Department of Chemical and Biomolecular Engineering, University of Akron, Akron, Ohio 44325, United States

Supporting Information

ABSTRACT: Forming core–shell and alloy structures offers generally two ways to design efficient Pt-based catalysts for oxygen reduction reaction (ORR). Here, we combined these two strategies and invented a versatile aqueous route to synthesize octahedral Pd@$Pt_{1.8}$Ni core–shell nanocrystals. The Pt/Ni atomic ratios in the resultant shells can be varied from 0.6 to 1.8, simply by changing the amounts of Pt and Ni precursors, with the other conditions unchanged. Experimental studies showed that the mass activities of as-prepared catalysts were 5 times higher than that of the commercial Pt/C. We believe that the ultrathin PtNi shells enclosed by {111} facets made it possible to reduce the Pt content while retaining the catalytic activity toward ORR. This strategy may be extended to the preparation of other multimetallic nanocrystals with shaped and ultrathin alloy shells, which is conducive to design highly active catalysts.

Proton-exchange membrane fuel cells are expected to work as a clean power source to replace increasingly scarce fossil fuels. However, they are still difficult to commercialize on a large scale, mainly owing to the challenge of developing active and economical electrocatalysts to mitigate the sluggish kinetics of the oxygen reduction reaction (ORR) at the cathode. Although platinum is proved to be the most effective catalyst among all the pure metals, high cost and scarcity limit its extensive use in industrial catalysts.[1] To maximize the utilization efficiency of Pt, massive efforts have been made.[2−5] One of the most promising methods is to synthesize core–shell structures by replacing the bulk of Pt with a less expensive metal. Palladium has been widely employed as a suitable substrate for the deposition of Pt, which was attributed to the close lattice match between Pd and Pt (lattice mismatch of only 0.77%).[6,7] Electronic coupling between Pd cores and Pt shells would endow these nanocrystals with enhanced ORR activity and durability compared with pure Pt catalysts. Xia and co-workers have successfully prepared Pd@Pt core–shell nanocrystals with improved ORR activity by coating Pd nanocrystals with well-controlled atomic layers of Pt.[8] Similar structures were also achieved by Adzic and co-workers, who deposited Pt monolayer on Pd-based nanocrystals through the galvanic replacement reaction between an underpotentially deposited Cu monolayer and Pt.[9−12] Another elegant approach is to employ a 3d transition metal (Ni, Cu, Co, and so on) to form alloy nanocrystals with certain facets. Owing to the exposed facets and synergistic effect, the as-prepared nanocrystals possess superior ORR activity.[13] Stamenkovic et al. observed that the ORR activity on the single-crystal $Pt_3Ni(111)$ surfaces was 90-fold higher than that of the commercial Pt/C catalysts.[14] Since then, a number of groups have prepared shaped PtNi nanocrystals enclosed by {111} facets to pursue an enhanced electrocatalytic performance.[15−21]

In this work, we combine the benefits of these two strategies and demonstrate a facile aqueous method to synthesize ∼28 nm octahedral Pd@$Pt_{1.8}$Ni core–shell nanocrystals. Specifically, the products were obtained by depositing approximately four atomic layers of PtNi alloy on the surface of Pd nanocrystals. Controllable Pt/Ni atomic ratios in the shells from 0.6 to 1.8 were successfully achieved by simply varying the amounts of Pt and Ni precursors added into the system. The ultrathin PtNi alloy skins of only a few atomic layers can largely increase the utilization efficiency and thereby minimize the use of Pt. Relative to the state-of-the-art Pt/C catalyst, the as-prepared Pd@Pt–Ni/C catalysts exhibited a mass ORR activity enhanced by 5-fold.

In a typical synthesis of octahedral Pd@$Pt_{1.8}$Ni core–shell nanocrystals, octahedral Pd nanocrystals served as the seeds, which were prepared through controlling the overgrowth of Pd nanocubes according to previous work.[22] Figure S1 (Supporting Information) shows transmission electron microscopy (TEM) images and the size distributions of Pd nanocubes and octahedrons, respectively. It can be clearly seen that both polyhedrons have a well-defined and uniform shape (Figure S1A,C). The size distributions were determined to be 11.1 ± 3.1 nm for Pd nanocubes (Figure S1B) and 25.9 ± 2.6 nm for Pd octahedrons (Figure S1D), respectively. The Pd octahedrons were then added into an aqueous solution containing hydrazine hydrate ($N_2H_4·H_2O$), citric acid monohydrate ($C_6H_8O_7·H_2O$), and poly(vinylpyrrolidone) (PVP, $M_w \approx$ 55 000). After the suspension was preheated at 65 °C under magnetic stirring for 5 min, a solution of an accurate amount of K_2PtCl_4 and $NiCl_2·6H_2O$ was slowly injected into the vial. The

Received: November 11, 2014
Published: February 12, 2015

DOI: 10.1021/ja511596c
J. Am. Chem. Soc. 2015, 137, 2804−2807

octahedral Pd@$Pt_{1.8}$Ni nanocrystals were obtained after the reaction had proceeded for another 15 min at 65 °C.

Figure 1A shows a bright-field TEM image of the resultant octahedral Pd@$Pt_{1.8}$Ni nanocrystals with an average edge length of ~28 nm, indicating a good morphological uniformity and high purity. The high-angle annular dark-field scanning TEM (HAADF-STEM, Figure 1B) image shows a clear contrast between the shell and the core due to the difference in atomic number between Pd and Pt. The Pd cores retained their original octahedral shape, indicating that they were intact during the deposition. The inset shows the corresponding selected area electron diffraction (SAED) pattern recorded along the [011] zone axis, which proves a high quality of single crystallinity. Figure 1C,D shows HAADF-STEM images of the regions marked by boxes in Figure 1B, which were taken along the [011] zone axis. The lattice spacings of 2.3 and 1.9 Å can be indexed to {111} and {200} planes, respectively. Additional HAADF-STEM images taken from different regions were integrated in Figure S2, supporting the unique octahedral core–shell nanostructure with an ultrathin PtNi shell composed of approximately four atomic layers. Figure 1E shows STEM energy-dispersive X-ray (STEM-EDX) elemental mapping images of Pd, Pt, and Ni, respectively, which were induced on the STEM image in Figure 1B.The main distribution of Pd in the interior supports pure Pd for the core, and the full coverage of both Pt and Ni reveals an alloy structure for the shell. From the energy dispersive X-ray (EDX) spectrum in Figure S3, Pd, Pt, and Ni signals can be observed, confirming the existence of these three elements. Figure 1F shows the line-scanning profiling analysis taken along the dotted line marked in Figure 1B, indicating a Pd-rich core and a PtNi alloy shell as well. The Pt/Ni atomic ratio was determined to be 1.8 according to inductively coupled plasma-atomic emission spectroscopy (ICP-AES) analysis.

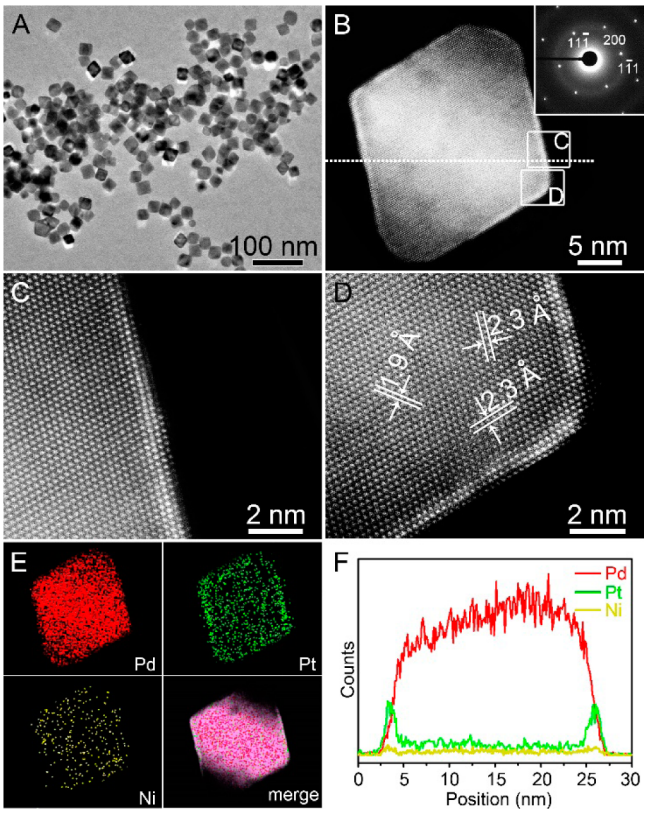

Figure 1. (A) Bright-field TEM image of octahedral Pd@$Pt_{1.8}$Ni core–shell nanocrystals. (B) HAADF-STEM image of an individual octahedral Pd@$Pt_{1.8}$Ni core–shell nanocrystal. The inset shows the corresponding SAED pattern. (C,D) Corresponding HAADF-STEM images of the regions marked in B. (E) STEM-EDX elemental mapping images of Pd, Pt and Ni and the merged image. (F) Elemental line-scanning profiles along the direction marked by a white line in B.

For Pt-based bimetallic nanocrystals, their physicochemical properties, including ORR activities, are known to be highly dependent on the elemental composition. Therefore, we added different amounts of precursors without changing the other conditions in order to tune Pt/Ni atomic ratio (x) of the resultant octahedral Pd@Pt_xNi nanocrystals. As the molar percentage of $NiCl_2$ added into the reaction mixture varies from 8.8 to 11, 15.6, and 25, x will vary from 1.8 to 1.5, 1.2, and 0.6, respectively. As shown in Figure S4, the morphology of obtained nanocrystals was barely changed although the molar percentage of Ni was different. The X-ray diffraction (XRD) patterns of all the octahedral Pd@Pt_xNi nanocrystals (x = 0.6, 1.2, 1.5, 1.8) in Figure S4D can be indexed as a face-centered-cubic (fcc) structure. No obvious peak shift was observed in comparison with fcc Pd, indicating the epitaxial deposition of ultrathin PtNi shells.

The electrocatalytic ORR properties of as-obtained octahedral Pd@$Pt_{1.8}$Ni nanocrystals were measured and compared with the commercial Pt/C (20 wt % loading, Johnson Matthey). Before deposited on rotating disk electrodes, the nanocrystals were loaded on Vulcan XC-72 carbon supports, and then treated with acetic acid at 70 °C for 2 h to clean the surface.[23,24] In view of the fact that the Pt/Ni ratio could be changed due to the leaching of Ni, the resultant catalysts are collectively called "Pd@Pt–Ni/C" in our discussion. Cyclic voltammograms (CVs) in the potential range of 0.05–1.05 V versus reversible hydrogen electrode (RHE) were obtained in a N_2-saturated 0.1 M $HClO_4$ solution at a sweep rate of 50 mV/s (Figure 2A). A slight positive shift of the onset potential of oxide reduction peak was observed for Pd@Pt–Ni/C comparing with Pt/C, which might result from the decrease of the deposition free energy of Pt–OH, Pt–O, or Pt–O_2 species caused by the effect of alloy Ni in the shells.[25] Through measuring the charge collected in the H_{upd} adsorption/desorption region after double-layer correction (Figure S5A) and assuming a value of 210 $\mu C/cm^2$ for the adsorption of a hydrogen monolayer, the electrochemical active surface area (ECSA) of Pd@Pt–Ni/C was calculated to be 4.29 cm^2, which is approximately 1.67 times greater than that of Pt/C (2.57 cm^2). As shown in Figure S5B, the specific ECSA (the ECSA per unit weight of metal) of Pd@Pt–Ni/C (178.01 m^2/g_{Pt}) was much higher than that of Pt/C (64.25 m^2/g_{Pt}), suggesting an increase in the utilization efficiency of Pt.

A series of ORR measurements were performed in an O_2-saturated 0.1 M $HClO_4$ solution at 10 mV/s at room temperature with a Pt loading of 12.3 $\mu g/cm^{-2}$ for Pd@Pt–Ni/C and 20.4 $\mu g/cm^{-2}$ for the commercial Pt/C. Figure 2B shows the positive-going ORR polarization curves of Pd@Pt–Ni/C and Pt/C. To better understand the mass and surface effects, we normalized the kinetic current calculated from the ORR polarization curve to the Pt mass and ECSA, respectively. As illustrated in Figure2C, the specific activity of Pd@Pt–Ni/C was obviously enhanced in the potential region between 0.85 and 0.96 V relative to the commercial Pt/C, demonstrating the

DOI: 10.1021/ja511596c
J. Am. Chem. Soc. 2015, 137, 2804–2807

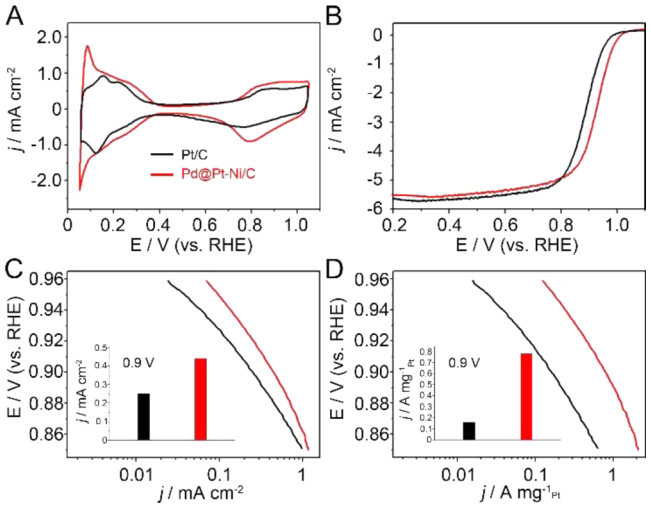

Figure 2. Comparison of electrocatalytic properties between Pd@Pt−Ni/C and the commercial Pt/C. (A) CV curves recorded at room temperature in a N_2-purged 0.1 M $HClO_4$ solution with a sweep rate of 50 mV/s. (B) Corresponding ORR polarization curves recorded in an O_2-saturated 0.1 M $HClO_4$ solution with a sweep rate of 10 mV/s and a rotation rate of 1600 rpm. (C) Specific and (D) mass activities given as kinetic current densities normalized to ECSA and Pt loading of the catalysts, respectively.

accelerated ORR kinetics on the surface of Pd@Pt−Ni/C. Figure 2D shows the Pt mass activity of Pd@Pt−Ni/C compared with that of Pt/C. It can be seen that a mass activity of 0.79 A/mg_{Pt} for Pd@Pt−Ni/C was 4.9 times higher than that of Pt/C (0.16 A/mg_{Pt}) at 0.9 V. In addition, based on the total mass of Pd and Pt, Pd@Pt−Ni/C exhibited a mass activity of 0.48 A/mg_{Pd+Pt}. The enhancement on the catalytic performance could be attributed to two factors: (i) increasement of Pt active sites because of the alloy of Pt with Ni, which could weaken the binding of oxygenated spectator species to Pt,[26] and (ii) interfacial interactions between the thin shell and the Pd core, which may modify the electronic and geometric structures of shell atoms.[27] Furthermore, to investigate composition-dependent ORR catalytic properties, Pd@Pt_xNi with other Pt/Ni atomic ratios (x = 0.6, 1.2, and 1.5) were also employed as electrocatalysts. Before ORR meaurements, all Pd@Pt_xNi underwent the same pretreatments (loading on carbon, treatment with acetic acid, followed by deposition on rotating disk electrodes) as Pd@$Pt_{1.8}$Ni did. The measurements indicate a trend that ORR activity of the electrocatalysts increases monotonically, with x rising from 0.6 to 1.8 (Figure S6).

To evaluate the durability of the Pd@Pt−Ni/C catalysts for ORR, we applied cyclic potential sweeps between 0.6 and 1.05 V at a sweep rate of 50 mV/s in a N_2-saturated 0.1 M $HClO_4$ solution (Figure S7). As shown in Figure 3A, Pd@Pt−Ni/C showed a slight loss of 6.7% in ECSA after 4000 cycles, while the commercial Pt/C showed a significant loss of 22%. After 6,000 cycles, the CV measurements showed a spot of drop of only 10% in ECSA for Pd@Pt−Ni/C, but a substantial loss of 27% for Pt/C, suggesting that the Pd@Pt−Ni/C had a better durability than the Pt/C catalysts. TEM analysis in Figure S8 reveals much slighter sintering and aggregation for Pd@Pt−Ni/C comparing with Pt/C (Figure S9) after 6000 cycles. This result is in accordance with a previous work, which could be attributed to the anchor effect that the mobility of Pt on carbon is hindered when Ni is present. Thus, a suppressed sintering

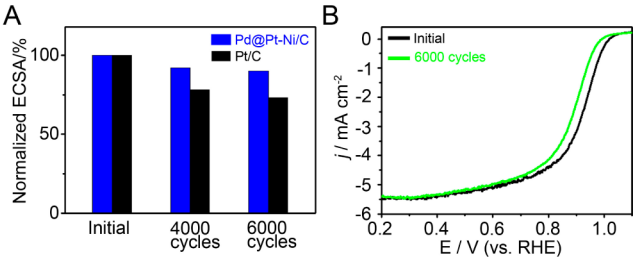

Figure 3. Electrochemical durability of the Pd@Pt−Ni/C and the commercial Pt/C. (A) Loss of ECSA for Pd@Pt−Ni/C and the commercial Pt/C after long-term potential sweep cycles. (B) ORR polarization curves of Pd@Pt−Ni/C before and after the durability test.

effect of Pt atoms was observed when compared with the case of Pt/C.[28]

The ORR polarization curves of Pd@Pt−Ni/C before and after the durability test are shown in Figure 3B. It should be pointed out that the ORR catalytic activity showed a typical degradation over extended test times, which may arise from the dealloying of PtNi with Ni leaching during the long-term test.[29−32] In order to verify the conjecture, we measured the content of Ni during the whole process. As shown in Figure S10, the atomic percentage of Ni was decreased by approximately 10% throughout the 6000 cycles, which indicates the existence of dealloying.

In summary, we have demonstrated an aqueous method to synthesize octahedral Pd@$Pt_{1.8}$Ni nanocrystals with an ultrathin PtNi alloy shell composed of approximately four atomic layers. The Pt/Ni atomic ratio in the resultant shells could be adjusted in the range of 0.6−1.8 by using this method. A range of electrochemical measurements reveal that the as-obtained Pd@$Pt_{1.8}$Ni nanocrystals exhibit better ORR activity and durability than the commercial Pt/C. We believe that this synthetic strategy may be extended to the preparation of other multimetallic nanocrystals with shaped alloy shells, making it possible to design highly active catalysts beyond fuel cell applications.

■ ASSOCIATED CONTENT

Ⓢ Supporting Information

Detailed synthesis, characterization results, and additional electrochemical data. This material is available free of charge via the Internet at http://pubs.acs.org.

■ AUTHOR INFORMATION

Corresponding Authors

*zpeng@uakron.edu
*zengj@ustc.edu.cn

Notes

The authors declare no competing financial interest.

■ ACKNOWLEDGMENTS

This work was supported by Collaborative Innovation Center of Suzhou Nano Science and Technology, MOST of China (2014CB932700 and 2011CB921403), 2015SRG-HSC049, NSFC under Grant Nos. 21203173, 51371164, 51132007 and J1030412, Strategic Priority Research Program B of the CAS under Grant No. XDB01020000, and Fundamental Research Funds for the Central Universities (WK2340000050, WK3510000002 and WK2060190025).

DOI: 10.1021/ja511596c
J. Am. Chem. Soc. 2015, 137, 2804−2807

REFERENCES

(1) Su, L.; Jia, W. Z.; Li, C.-M.; Lei, Y. *ChemSusChem* **2014**, *7*, 361.
(2) Bing, Y. H.; Liu, H. S.; Zhang, L.; Ghosh, D.; Zhang, J. J. *Chem. Soc. Rev.* **2010**, 392184.
(3) Gan, L.; Heggen, M.; Rudi, S.; Strasser, P. *Nano Lett.* **2012**, *12*, 5423.
(4) Wu, B. H.; Zheng, N. F. *Nano Today* **2013**, *8*, 168.
(5) Jackson, A.; Viswanathan, V.; Forman, A. J.; Larsen, A. H.; Norskov, J. K.; Jaramillo, T. F. *ChemElectroChem* **2014**, *1*, 67.
(6) Zhang, H.; Jin, M. S.; Wang, J. G.; Kim, M. J.; Yang, D.; Xia, Y. N. *J. Am. Chem. Soc.* **2011**, *133*, 10422.
(7) Shao, M. H.; He, G. N.; Peles, A.; Odell, J. H.; Zeng, J.; Su, D.; Tao, J.; Yu, T.; Zhu, Y.; Xia, Y. N. *Chem. Commun.* **2013**, *49*, 9030.
(8) Xie, S. F.; Choi, S.-I.; Liu, N.; Roling, L. T.; Herron, J. A.; Zhang, L.; Park, J.; Wang, J. G.; Kim, M. J.; Xie, Z. X.; Mavrikakis, M.; Xia, Y. N. *Nano Lett.* **2014**, *14*, 3570.
(9) Zhang, J. L.; Vukmirovic, M. B.; Xu, Y.; Mavrikakis, M.; Adzic, R. R. *Angew. Chem., Int. Ed.* **2005**, *44*, 2132.
(10) Knupp, S. L.; Vukmirovic, M. B.; Haldar, P.; Herron, J. A.; Mavrikakis, M.; Adzic, R. R. *Electrocatalysis* **2010**, *1*, 213.
(11) Kuttiyiel, K. A.; Sasaki, K.; Su, D.; Vukmirovic, M. B.; Marinkovic, N. S.; Adzic, R. R. *Electrochim. Acta* **2013**, *110*, 267.
(12) Sasaki, K.; Naohara, H.; Choi, Y. M.; Cai, Y.; Chen, W.-F.; Liu, P.; Adzic, R. R. *Nat. Commun.* **2012**, *3*, 1115.
(13) Wu, Y.; Cai, S. F.; Wang, D. S.; He, W.; Li, Y. D. *J. Am. Chem. Soc.* **2012**, *134*, 8975.
(14) Stamenkovic, V. R.; Fowler, B.; Mun, B. S.; Wang, G. F.; Ross, P. N.; Lucas, C. A.; Markovic, N. M. *Science* **2007**, *315*, 493.
(15) Wu, J. B.; Gross, A.; Yang, H. *Nano Lett.* **2011**, *11*, 798.
(16) Wu, J. B.; Qi, L.; You, H. J.; Gross, A.; Li, J.; Yang, H. *J. Am. Chem. Soc.* **2012**, *134*, 11880.
(17) Cui, C. H.; Gan, L.; Li, H.-H.; Yu, S.-H.; Heggen, M.; Strasser, P. *Nano Lett.* **2012**, *12*, 5885.
(18) Chen, C.; Kang, Y. J.; Huo, Z. Y.; Zhu, Z. W.; Huang, W. Y.; Xin, H. L. L.; Snyder, J. D.; Li, D. G.; Herron, J. A.; Mavrikakis, M.; Chi, M. F.; More, K. L.; Li, Y. D.; Markovic, N. M.; Somorjai, G. A.; Yang, P. D.; Stamenkovic, V. R. *Science* **2014**, *343*, 1339.
(19) Cui, C. H.; Gan, L.; Heggen, M.; Rudi, S.; Strasser, P. *Nat. Mater.* **2013**, *12*, 765.
(20) Zhang, J.; Yang, H. Z.; Fang, J. Y.; Zou, S. Z. *Nano Lett.* **2010**, *10*, 638.
(21) Carpenter, M. K.; Moylan, T. E.; Kukreja, R. S.; Atwan, M. H.; Tessema, M. M. *J. Am. Chem. Soc.* **2012**, *134*, 8535.
(22) Jin, M. S.; Zhang, H.; Xie, Z. X.; Xia, Y. N. *Energy Environ. Sci.* **2012**, *5*, 6352.
(23) Choi, S.-I.; Xie, S. F.; Shao, M. H.; Odell, J. H.; Lu, N.; Peng, H.-C.; Protsailo, L.; Guerrero, S.; Park, J.; Xia, X. H.; Wang, J. G.; Kim, M. J.; Xia, Y. N. *Nano Lett.* **2013**, *13*, 3420.
(24) Mazumder, V.; Sun, S. H. *J. Am. Chem. Soc.* **2009**, *131*, 4588.
(25) Zhang, K.; Yue, Q. L.; Chen, G. F.; Zhai, Y. L.; Wang, L.; Wang, H. S.; Zhao, J. S.; Liu, J. F.; Jia, J. B.; Li, H. B. *J. Phys. Chem. C* **2011**, *115*, 379.
(26) Wang, C.; Markovic, N. M.; Stamenkovic, V. R. *ACS Catal.* **2012**, *2*, 891.
(27) Mazumder, V.; Chi, M. F.; More, K. L.; Sun, S. H. *J. Am. Chem. Soc.* **2010**, *132*, 7848.
(28) Colon-Mercado, H. R.; Kim, H. S.; Popov, B. N. *Electrochem. Commun.* **2004**, *6*, 795.
(29) Cui, C. H.; Gan, L.; Neumann, M.; Heggen, M.; Cuenya, B. R.; Strasser, P. *J. Am. Chem. Soc.* **2014**, *136*, 4813.
(30) Fernandes, A. C.; Paganin, V. A.; Ticianeli, E. A. *J. Electroanal. Chem.* **2010**, *648*, 156.
(31) Mayrhofer, K. J. J.; Hartl, K.; Juhart, V.; Arenz, M. *J. Am. Chem. Soc.* **2009**, *131*, 16348.
(32) Nikkuni, F. R.; Ticianelli, E. A.; Dubau, L.; Chatenet, M. *Electrocatalysis* **2013**, *4*, 104.

DOI: 10.1021/ja511596c
J. Am. Chem. Soc. 2015, 137, 2804−2807